Synergism of Porphyrin-Core Saddling and Twisting of *meso*-Aryl Substituents

Angela Rosa,*,§ Giampaolo Ricciardi,*,§ and Evert Jan Baerends*,‡

Dipartimento di Chimica, Università della Basilicata, Via N. Sauro 85, 85100 Potenza, Italy, and Afdeling Theoretische Chemie, Vrije Universiteit, De Boelelaan 1083, 1081 HV Amsterdam, The Netherlands

Received: February 13, 2006; In Final Form: February 27, 2006

The structural chemistry of *meso*-aryl-substituted porhyrins has uncovered a bewildering variety of macrocycle distortions. Saddling angles range up to 40°, while the plane of the phenyl groups at the meso positions may be anywhere between perpendicular to the porphyrin plane ($\theta = 90°$) and tilted to quite acute angles ($\theta =$ 30° or even less). These two distortions appear to be correlated. This has naturally been explained by steric hindrance: when the phenyls rotate toward the porphyrin plane, for instance, coerced by packing forces, the pyrrole rings can alleviate the steric hindrance by tilting away to a saddled conformation. We demonstrate, however, that the two motions are intrinsically coupled by electronic factors and are correlated even in the absence of external forces. A saddling motion makes it sterically possible for the phenyl rings to rotate toward the porphyrin plane, which will always happen because of increasingly favorable π-conjugation interaction with smaller angles θ. The considerable energy lowering due to π conjugation counteracts the energy cost of the saddling, making the concerted saddling/rotation motion very soft. Unsubstituted *meso*-aryl porphyrins just do not distort, but an additional driving force may tip the balance in favor of the combined distortion motion. Internal forces having this effect are repulsion of the four hydrogens that occupy the central hole of the ring in porphyrin diacids but also steric repulsion in peripherally crowded porphyrins. These findings lead to a clarification and systematization of the observed structural variety, which indeed shows a remarkable correlation between saddling and phenyl ring tilting.

Introduction

Conformationally distorted porphyrins have been extensively studied in recent years. The great importance of the macrocycle nonplanarity for biological functions motivated the initial interest,[1] which has been subsequently enlarged by their potential in nonbiological applications, such as supramolecular chemistry[2,3] and catalysis.[4]

We will be focusing in this paper on the so-called saddling distortion, which consists of the simultaneous tilting upward of two opposite pyrrole rings and the tilting downward of the two other opposite pyrrole rings (see Figure 1). The degree of saddling projections can be defined by the saddling angle φ that a pyrrole ring makes with the porphyrin plane. The saddling distortion may or may not be coupled with a rotation of *meso*-phenyl rings (rotation around the C_m-C_1 bond; see Figure 1). This rotation is described by the angle θ between the phenyl plane and the porphyrin plane.

There is by now a large body of detailed structural chemistry of saddled *meso*-aryl-containing porphyrins.[5] This has revealed a bewildering variation in the extent to which distortions occur: the φ angles may vary over a wide range (from 0° up to 40°), and θ may go down from 90° to angles below 30°. It is not easy to see a pattern in these data because there are important effects on the magnitude of these conformational distortions coming from other structural features, such as the orientation of axial ligands in metal derivatives,[6,7] steric crowding due to bulky peripheral substituents, as in the dodeca-substituted porphyrins,[8−13] or two additional protons in the porphyrin core, as in the diacids.[5,14−16] The magnitude of the various steric repulsions is however unknown, as is the strain caused by the distortions.

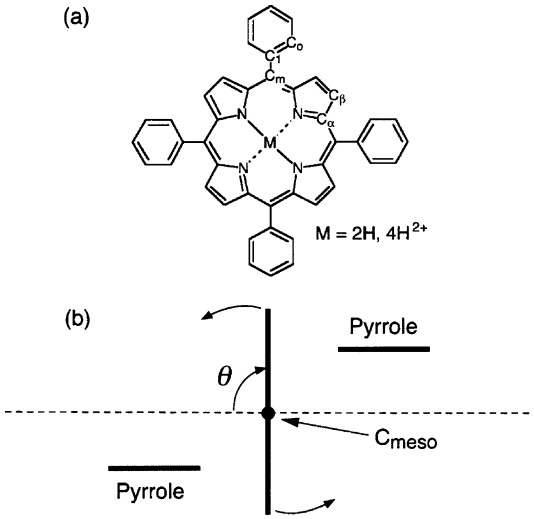

Figure 1. (a) Labeling of the various carbon atoms in tetraphenylporphyrin. (b) Definition of rotation angle θ of the phenyl plane between an upward-tilted pyrrole (to its right) and a downward-tilted pyrrole (to its left). The view is toward the porphyrin center; the plane of the drawing is the plane perpendicular to the porphyrin plane and the C_1-C_m axis, through C_m.

A careful inspection of the available structural data suggests that *meso*-aryl substituents play a special role in the porphyrin distortions. Just a tetraphenyl substitution at the meso carbons does not induce a distortion; compare the essentially planar H_2TPP (*meso*-tetraphenylporphyrin).[17−19] However, this substitution appears to enhance the distorting effect of other steric repulsions such as those coming from bulky peripheral substit-

* E-mail: rosa@unibas.it; rg010sci@unibas.it; baerends@few.vu.nl.
§ Università della Basilicata.
‡ Vrije Universiteit.

10.1021/jp060931i CCC: $33.50
Published on Web 03/30/2006

uents or the inner hydrogens in the diacids. As a matter of fact, the deviation from planarity for diacids bearing *meso*-aryl substituents, such as H_4TPP^{2+} (*meso*-tetraphenylporphyrin) and H_4TPyP^{2+} [*meso*-tetrakis(4-pyridyl)porphyrin] is much more pronounced[14,16] than that for other diacids, such as H_4OEP^{2+} (octaethylporphyrin).[16,20] For instance, in H_4TPP^{2+} derivatives, the average tilt of the pyrrole rings from the 24-atom mean plane, φ, ranges between 28 and 33°,[14,16,21] which is to be compared to the $\varphi \sim 14°$ value seen in H_4OEP^{2+} derivatives.[16,20]

Similarly, peripherally crowded *meso*-tetraphenylporphyrins such as H_2DDPP (2,3,7,8,10,12,13,15,17,18,20-dodecaphenylporphyrin)[10] and H_2OETPP (2,3,7,8,12,13,17,18-octaethyl-5,10,15,20-tetraphenylporphyrin)[22] show deviations from planarity that are even somewhat larger than those for *meso*-aryl-containing diacids. The diacids of these highly substituted porphyrins exhibit even larger distortions (saddling).[23,24]

Saddled *meso*-arylporphyrins usually display quite acute aryl-porphyrin dihedral angles ($\theta < 60°$), with the magnitude of θ being directly related to the extent of the *sad* distortion: more acute aryl-porphyrin dihedral angles correlate with larger degrees of saddling.[6,7,16] As an example, in $[H_4TPP](ClO_4)_2$, where the average porphyrin−aryl dihedral angle, θ, is 27(2)°, the absolute displacement of the pyrrole β-carbon atoms from the porphyrin plane, $|\Delta C_\beta|$, which can be considered as an alternative measure of the deviation from planarity, amounts to 0.93(6) Å,[16] whereas in $[H_4TMP](ClO_4)_2$ (TMP = tetramesitylporphyrin), where θ is ca. 60°, $|\Delta C_\beta|$ is 0.67 Å,[16] i.e., only 0.20 Å larger than that in $[H_4OEP](ClO_4)_2$,[16] a diacid which lacks aryl groups.

The observed correlation between the saddling distortion of the porphyrin core and the tilting of the *meso*-aryl substituents has been explained so far in terms of *environmental effects* (see ref 16 and references cited therein). On the basis of detailed structural analyses and molecular mechanics (MM) calculations, it was argued that the saddle distortion increases with a decrease in the porphyrin−aryl dihedral angle to minimize the repulsive steric interactions between the tilted aryl substituents and the CH groups of the flanking pyrrole rings, the driving force for the tipping over of the *meso*-aryl substituents coming from *environmental factors* such as packing forces in the solid state. It seemed plausible to assume that the tilting of the *meso*-aryl groups was primarily dictated by environmental factors because the MM-calculated structures were not able to reproduce the experimentally observed aryl−porphyrin dihedral angles, which were in general considerably underestimated.[7,16] On the other hand, there was little reason to trace the discrepancy between the experimental and calculated θ values to a failure of the MM calculations because these were able to reproduce the experimental degree of saddling when the aryl group orientations were constrained at their X-ray values, i.e., when packing forces were supposedly taken into account.[16]

Our recent density functional theory (DFT) calculations of the molecular structures of a series of *meso*-tetraphenylporphyrin diacids, $[H_4TPP](X)_2$ (X = F, Cl, Br, I),[25] suggest, however, that the environment plays only a very minor role, if any, in determining the orientations of the aryl rings. Indeed, the calculations correctly predict the degree of tilting of the phenyl groups as well as the type and degree of distortion of the porphyrin core. The nice agreement between the calculated "gas-phase" conformations and the solid-state structures implies that the saddling distortion of the porphyrin core and the tilting of the *meso*-aryl groups are coupled through a synergic mechanism that is entirely governed by *intrinsic electronic factors*.

Drawing definite conclusions on the interrelationship of these two motions would be highly desirable also in view of the design of macrocycles with predefined conformations.

It is the purpose of this work to clarify and quantify the electronic factors governing this *synergic* mechanism.

To this end, we have studied theoretically, by a DFT approach, the saddling motion of the porphyrin core, coupled and uncoupled with the tilting motion of the *meso*-aryl groups. Energetic information (magnitude of strain and of steric repulsion) is obtained by computing, for H_2TPP and its diacid derivative, H_4TPP^{2+}, the potential energy curves (PECs) along the saddling angle, φ, the tilting angle θ of the *meso*-aryl substituents, and combinations of the two coordinates. Insight into the electronic factors is obtained by way of an energy decomposition scheme (see the next section) combined with a fragment-oriented approach. We take as building blocks of H_2TPP and H_4TPP^{2+}, on the one hand, a porphyrin core bearing an unpaired electron on each bridging carbon atom, $[H_2(PyC^{\bullet})_4]$ or $[H_4(PyC^{\bullet})_4]^{2+}$, and, on the other hand, a cage of four phenyl groups, $(Ph^{\bullet})_4$. This allows us to analyze and quantify the electronic factors governing the porphyrin-core saddling and twisting of the phenyl groups and reveal any synergistic coupling between the two.

Method

General Procedures. All calculations have been performed with the program package ADF (Amsterdam Density Functional), version 2004.[26,27]

The calculations made use of the local density approximation functional of Vosko−Wilk−Nusair (VWN),[28] plus the generalized gradient approximation, employing Becke's[29] gradient approximation for exchange and Perdew's[30] for correlation (BP86).

The ADF TZ2P basis set, which is an uncontracted triple-ζ STO basis set with two polarization functions (H, 2p, 3d; C and N, 3d, 4f), was used. The cores (C and N, 1s) were kept frozen.

The PECs along the φ coordinate were computed for H_2P (P = porphine), H_2TPP, and their corresponding diacids, H_4P^{2+} and H_4TPP^{2+}, in the range of $\varphi = 0-40°$. At each φ value, all geometrical parameters were optimized within C_{2v} (H_2P and H_2TPP) or D_{2d} (H_4P^{2+} and H_4TPP^{2+}) symmetry constraints. During the optimization, the *meso*-phenyl groups were kept perpendicular to the mean porphyrin plane ($\theta = 90°$).

The PECs along the θ coordinate were computed for H_2TPP and H_4TPP^{2+}, in the range of $\theta = 0-90°$, for the planar and several saddle conformations. At each θ value, all geometrical parameters (except for the saddling angle, φ) were optimized within C_{2v} (H_2TPP) or D_{2d} (H_4TPP^{2+}) symmetry constraints.

Interaction Energy Analysis. To analyze and quantify the electronic factors governing the synergism of the porphyrin-core saddling and twisting of the phenyl groups in H_2TPP and H_4TPP^{2+}, we have used the energy-partitioning scheme of ADF,[27,31] which was originally developed for Hartree−Fock wave functions by Morokuma[32] and modified for the relaxation energy (or orbital interaction term) by Ziegler and Rauk.[33] The decomposition is for the interaction energy between a porphyrin core bearing an unpaired electron on each bridging carbon atom, $[H_2(PyC^{\bullet})_4]$ or $[H_4(PyC^{\bullet})_4]^{2+}$, and a cage of four phenyl groups, $(Ph^{\bullet})_4$. According to the energy-partitioning scheme, the interaction energy, ΔE_{int}, between fragments A and B is decomposed into a number of terms. The first term, $\Delta E°$, which is usually called the steric interaction energy, is obtained from the energy of the wave function ψ^0, which is constructed as the antisym-

metrized (*A*) and renormalized (*N*) product of the wave functions ψ^A and ψ^B of the fragments A and B:

$$\psi^0 = NA\{\psi^A\psi^B\} \qquad E^0 = \langle\psi^0|H|\psi^0\rangle \tag{1}$$

The $\Delta E°$ term, which is defined unambiguously as $\Delta E° = E° - E^A - E^B$, consists of two components, ΔV_{elstat} and ΔE_{Pauli}:

$$\Delta E° = \Delta V_{elstat} + \Delta E_{Pauli} \tag{2}$$

ΔV_{elstat} can be conceived as the classical electrostatic interaction of the nuclear charges and unperturbed electronic charge distribution of one fragment with those of the other fragment, with both fragments being at their final position. ΔV_{elstat} is usually negative, i.e., attractive. The second term in eq 2, ΔE_{Pauli}, refers to the repulsive interactions between the fragments, which are caused by the fact that two electrons with the same spin cannot occupy the same region in space. ΔE_{Pauli} is calculated by enforcing the Kohn−Sham determinant on the superimposed fragments to obey the Pauli principle by antisymmetrization and renormalization. The ΔE_{Pauli} term comprises the three- and four-electron destabilizing interactions between occupied orbitals and corresponds to the intuitive concept of steric repulsion[34−36] that is widely used in chemistry. The stabilizing orbital interaction term, ΔE_{oi}, is calculated in the final step of the energy-partitioning analysis when the Kohn−Sham orbitals relax to the fully converged ground-state wave function of the total molecule. This term accounts for charge transfer (interaction between occupied orbitals on one molecular fragment and unoccupied orbitals on the other) and polarization (empty/occupied orbital mixing on one fragment).[32] In the case of open-shell fragments, ΔE_{oi}, in addition to the charge-transfer and polarization energies, also contains the energy lowering connected to the formation of the electron-pair bonds, i.e., the energy gained by pairing the open-shell electrons in the bonding combination of the orbitals.

The ΔE_{oi} term may be broken up into contributions from the orbital interactions within the various irreducible representations Γ of the overall symmetry group of the system:[33]

$$\Delta E_{oi} = \sum_{\Gamma} \Delta E(\Gamma) \tag{3}$$

This decomposition scheme of the ΔE_{oi} term has been extensively used in this paper to analyze the attractive contributions to the interactions mentioned above.

Electron-pair bonds, which are formed when the porphyrin core, $[H_2(PyC^{\bullet})_4]$ or $[H_4(PyC^{\bullet})_4]^{2+}$, interacts with the cage of four phenyl groups, $(Ph^{\bullet})_4$, are handled using an open-shell fragment procedure.[37]

The interaction energy analysis has been performed in the range of $\theta = 0-140°$ for two conformations of the porphyrin core, i.e., planar ($\varphi = 0°$) and saddled ($\varphi = 30°$). While θ is varied, the interacting fragments have been taken in the same geometry that they have in the planar and saddled structures of H_2TPP and H_4TPP^{2+} optimized with the $\theta = 90°$ constraint.

Saddling of the Porphyrin Core and Tilting of the *meso*-Aryl Groups: PECs

We first explore the energy changes related to two deformation modes of unsubstituted and *meso*-aryl-substituted porphyrins as well as their diacids. In particular, the saddling and the rotation of the phenyl rings around the C_m-C_1 axis, and their possible mutual influence, are studied. It will become clear that these deformations are connected, with the energy cost of the saddling being strongly diminished by simultaneous twisting of the phenyls. Next we will look for an electronic structure explanation of this remarkable effect of phenyl twisting.

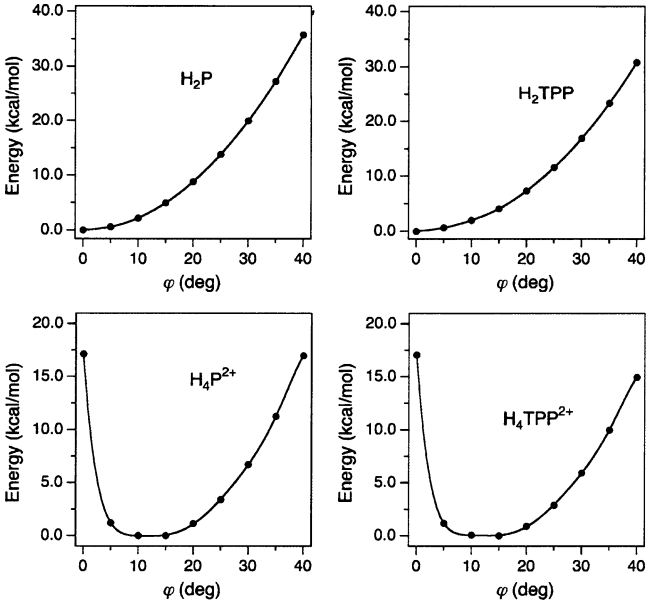

Figure 2. Potential energy variation along the saddling angle φ. The energies are given in units of kcal/mol with respect to the lowest-energy structures, i.e., D_{2h} planar with $\varphi = 0°$ for H_2P and H_2TPP and D_{2d} saddled with $\varphi = 15°$ for H_4P^{2+} and H_4TPP^{2+}.

Porphyrin-Core Saddling. We first investigate the energetics of the porphyrin-core saddling in cases where this motion does not couple with the tilting motion of the *meso*-aryl substituents. To this end, we have computed the PECs along the saddling coordinate, φ, for H_2TPP and its diacid derivative, H_4TPP^{2+}, keeping the *meso*-aryl substituents orthogonal to the mean porphyrin plane. We compare to H_2P and its diacid derivative, H_4P^{2+}, which lack *meso*-aryl substituents. The computed PECs are displayed in Figure 2.

Our first observation is that the overall shape of the PECs of tetraphenyl-substituted systems is remarkably similar to that of the unsubstituted systems. A careful inspection of the PECs in Figure 2 reveals that from $\varphi = 10°$ onward the H_2TPP PEC is somewhat less stiff than the H_2P PEC, and the same holds for H_4TPP^{2+} versus H_4P^{2+}. A plausible explanation is that in H_2TPP and H_4TPP^{2+} the energy cost of the saddling is partially compensated for by the relief of steric repulsion between $C_\beta-H$ σ bonds and the π system of the phenyl rings.

The main conclusion, however, is that the phenyl rings, when they are forced to be orthogonal to the mean porphyrin plane, as is the case here, have very little effect on the saddling motion.

We can therefore compare the free bases with the diacids, irrespective of the tetraphenyl substitution. As for the free bases, H_2P and H_2TPP, the PECs show that the porphyrin ring prefers to stay planar, although small distortions from planarity ($\varphi < 10°$) are energetically not very demanding, and slightly saddled conformations could be easily populated in the condensed phase. The preference for the planar conformation is understandable because the tilting motion of the pyrrole rings out of the porphyrin plane weakens the π conjugation between the pyrrole rings and the methine bridges. Indeed, as the plot of Figure 3 shows, in H_2P (and in H_2TPP, not shown), the overlap between the C_m and C_α $2p_\pi$ orbitals (kept orthogonal to the porphyrin plane, defined by the four C_m's, and to the pyrrole ring, respectively) decreases as φ increases. In the diacids, the trend is similar (see Figure 3), although there the overlap is invariably smaller than

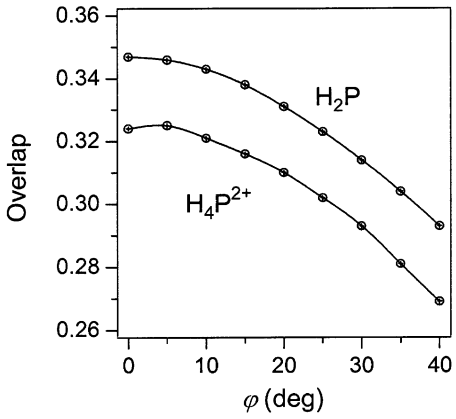

Figure 3. Variation of the overlap between the C_α and C_m $2p_\pi$ orbitals along the saddling angle φ.

that in the parent free bases, particularly at $\varphi = 0°$. This is because the repulsion of the inner hydrogens induces a significant expansion of the porphyrin core, especially at $\varphi = 0°$.

When looking at the PECs for the diacids, we note immediately that they are strikingly different from the free bases around $\varphi = 0°$. The potential energy is high at $\varphi = 0°$ but drops rapidly as soon as the saddling motion is turned on. This behavior is a direct consequence of the relief of repulsion of the inner hydrogens when the pyrrole rings are tilted up and down with respect to the mean porphyrin plane. In the range of $\varphi = 10-15°$, the relief of repulsion of the inner hydrogens is countered by the energy cost of the saddling and the PECs show a shallow minimum. At φ larger than 15°, the repulsion of the inner hydrogens has been totally relieved and the PECs of the diacids curve upward, just as those of the corresponding free bases do.

One may expect the PECs of peripherally crowded porphyrins, such as dodeca-substituted porphyrins, to show a qualitatively similar φ dependence as those of the diacids. Of course, in the peripherally crowded porphyrins, the canting of the pyrrole rings would serve to relieve the Pauli repulsion between the substituents at the C_β and C_m positions rather than between the inner hydrogens.

Two important conclusions can be drawn from the analysis of the saddling: (i) The energetics of the saddling is nearly insensitive to the presence of *meso*-aryl substituents, provided they are kept orthogonal to the porphyrin plane. (ii) For both diacids, H_4P^{2+} and H_4TPP^{2+}, a value of $\varphi \sim 15°$ is predicted as the upper limit for the saddling angle. This value practically coincides with that observed in porphyrin diacids lacking *meso*-phenyl substituents, such as H_4OEP^{2+}, and is only slightly smaller than that found in H_4TMP^{2+} ($\varphi \sim 20°$), a diacid where the observed porphyrin−aryl dihedral angle θ is smaller than 60°. These saddling angles are much smaller, however, than the $\varphi \sim 30°$ value observed in H_4TPP^{2+} and H_4TPyP^{2+} diacids, where at the same time the *meso*-aryl groups are tilted quite strongly.

These results clearly suggest that the tilting of the *meso*-aryl substituents does play a role in determining the actual degree of saddling observed in *meso*-aryl-containing diacids.

Coupling of the Saddling Distortion of the Porphyrin Core to the Tilting of the *meso*-Aryl Groups. To assess the relationship between the saddling distortion of the porphyrin core and the tilting of the *meso*-aryl substituents, we have computed the PECs along the θ coordinate for the planar and several saddled conformations of H_2TPP and its diacid derivative. These are displayed in Figures 4 and 5, respectively.

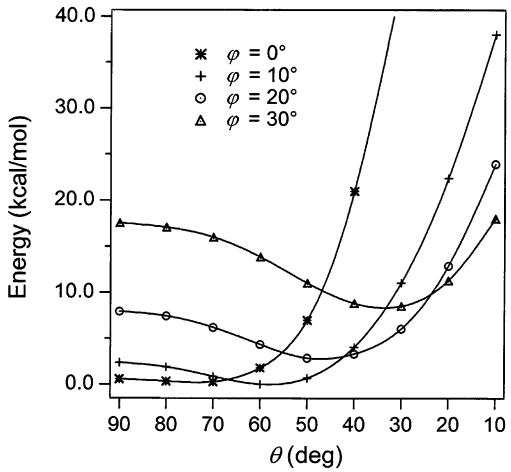

Figure 4. Potential energy variation along the tilting angle θ for planar and several saddled conformations of H_2TPP. The energies are given in units of kcal/mol with respect to the lowest-energy structure with $\varphi = 10°$ and $\theta = 60°$.

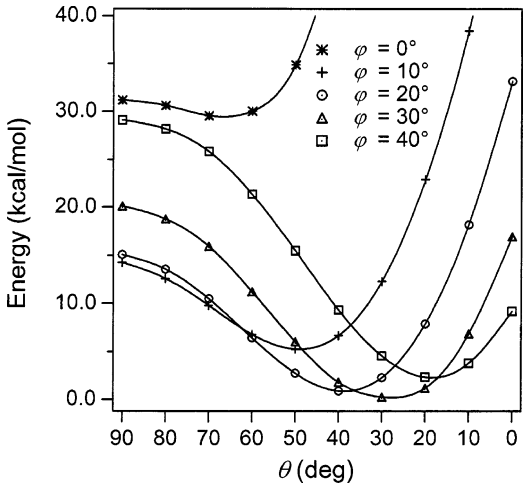

Figure 5. Potential energy variation along the tilting angle θ for planar and several saddled conformations of H_4TPP^{2+}. The energies are given in units of kcal/mol with respect to the lowest-energy structure with $\varphi = 30°$ and $\theta = 30°$.

When one considers tilting of the *meso*-phenyls in saddled porphyrins, the sense of rotation is important. In Figure 1b, the displacement of the two pyrrole rings adjacent to a given meso carbon is indicated by the raising and lowering of the projection of the $C_\beta-C_\beta$ bond on the plane of drawing, which is through the plane through C_m and perpendicular to the porphyrin plane and the C_1-C_m axis. The phenyl (indicated by its projection in the plane of drawing) can be rotated counterclockwise, which we indicate with decreasing θ angles (cf. the arrows), or clockwise, i.e., to larger θ values. Because of the D_{2d} symmetry, counterclockwise rotation of one phenyl implies clockwise rotation of the two neighboring phenyls. Evidently, clockwise rotation will be sterically not favorable, so the acute phenyl−porphyrin plane angles will occur in the counterclockwise rotation, which we will be dealing with unless stated explicitly otherwise.

Considering first H_2TPP (see Figure 4), we note that the PEC at $\varphi = 0°$ is nearly flat in the range of $\theta = 60-90°$ (a very shallow minimum is predicted at around 70°), indicating that the phenyl rings are nearly free to rotate about their bond to the porphyrin in this range of θ.

What we find fits in with X-ray structural data concerning *meso*-polyarylporphyrins, including H_2TPP, which show that in

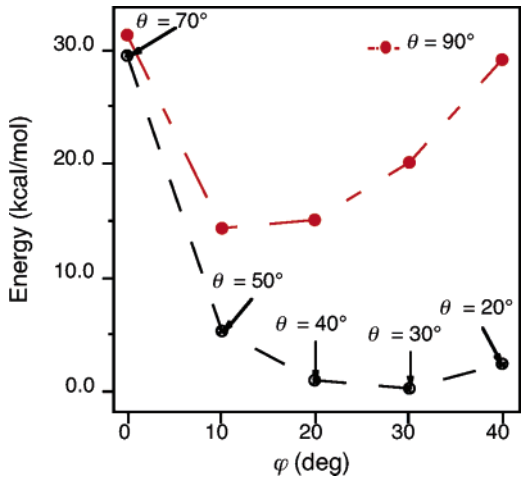

Figure 6. Potential energy variation along the saddling angle φ for H_4TPP^{2+} at $\theta = 90°$ (upper curve) and at the optimal θ values (lower curve). The energies are given in units of kcal/mol with respect to the lowest-energy structure with $\varphi = 30°$ and $\theta = 30°$.

these systems the dihedral angle between the plane of the porphyrin and the plane of the aryl is usually between 90° and 60°.[18,19,38−41] The rapid rise of the $\varphi = 0°$ PEC from $\theta \sim 60°$ onward indicates that θ can hardly become smaller than 60° if the porphyrin core stays planar. At variance with the $\varphi = 0°$ PEC, the PECs calculated for the saddled conformations of H_2TPP show a well-pronounced minimum at $\theta < 90°$. The optimal θ value varies with the degree of saddling. To a larger degree of saddling correspond smaller θ values.

Owing to the modest energy cost of the saddling, the minimum at $\theta = 60°$ on the $\varphi = 10°$ PEC turns out to be the overall minimum. Saddling distortions larger than 10° cost more energy to begin with, so the $\varphi = 20°$ and 30° PECs are destabilized with respect to the $\varphi = 10°$ PEC, and their minimum is higher than the overall minimum by ~2 and ~8 kcal/mol, respectively.

Coming now to the H_4TPP^{2+} PECs displayed in Figure 5, their behavior as a function of θ is qualitatively similar to that of the H_2TPP PECs, yielding energy lowering upon phenyl rotation, but the effect is more pronounced. The $\varphi = 0°$ PEC is again flat in the range of $\theta = 60-90°$ (a very shallow minimum is computed at $\theta \sim 70°$) and rises rapidly from $\theta = 60°$ onward, whereas the $\varphi > 0°$ PECs all have pronounced minima at $\theta < 90°$. Moreover, as inferred from the PECs in Figure 5 and more clearly from the $E(\varphi)$ curve of Figure 6, the optimal θ value shifts to smaller values as the degree of saddling increases.

The crucial difference between H_4TPP^{2+} and the parent free base is that in the former the saddling is energetically favorable to begin with (see Figure 2), so the $\varphi = 10°$ PEC is strongly stabilized with respect to the one for the planar ($\varphi = 0°$) H_4TPP^{2+}. For larger saddling angles, the energy goes up again (at $\theta = 90°$), although even at $\varphi = 40°$ the energy is still lower than that for the planar conformation. The energy cost of stronger saddling than $\varphi = 10°$ is overcompensated for by more pronounced energy lowering upon phenyl rotation, and the minimum at $\theta = 30°$ on the $\varphi = 30°$ PEC now becomes the overall minimum. We note, in passing, that the φ and θ values corresponding to the overall minimum in the explored range of θ and φ compare very well with those experimentally observed in H_2TPP diacids ($\varphi = 27.9-33°$; $\theta = 21-27°$)[14−16,23] and are nearly coincident with those theoretically predicted for the lowest-energy D_{2d} structure of H_4TPP^{2+} ($\varphi = 30.6°$; $\theta = 28.8°$).[25]

The above results demonstrate unequivocally that there is synergism between porphyrin-core saddling and tilting of the *meso*-aryl groups. This stands out when one compares (see Figure 6) the PEC for saddling with θ constrained to 90° (upper curve in Figure 6) to the PEC that is obtained when optimizing at each saddling angle the phenyl rotation angle (lower curve in Figure 6). Apparently, the phenyl rotation strongly assists in the saddling, and the total PEC becomes rather shallow for large saddling angles (φ in the range 15−40°) when the phenyl rotation is allowed to exert its energy-lowering effect. It is just the synergism of saddling and phenyl rotation that accounts for the remarkable flexibility (softness in the concerted saddling/tilting motion) of *meso*-aryl-containing porphyrins and for the enhanced saddling distortion observed in *meso*-aryl-containing porphyrin diacids.

These findings call for a reassessment of the accepted view that the enhanced saddling distortion observed in *meso*-aryl-containing porphyrins is simply due to relief of steric repulsion with the *meso*-aryl groups when the latter are forced to tilt by environmental effects.

Electronic Origins of the Synergism of Porphyrin-Core Saddling and Tilting of the *meso*-Aryl Groups

To understand the electronic factors governing the mutual influence of porphyrin-core saddling and twisting of the phenyl groups, we have performed an energy decomposition analysis of the interaction between a porphyrin core bearing an unpaired electron on each bridging carbon atom, $[H_2(PyC^{\bullet})_4]$ for H_2TPP, $[H_4(PyC^{\bullet})_4]^{2+}$ for H_4TPP^{2+}, and a cage of four phenyl groups, $(Ph^{\bullet})_4$. This analysis has been performed for different orientations of the phenyl groups and for two conformations of the porphyrin core, i.e., planar ($\varphi = 0°$) and saddled ($\varphi = 30°$).

The orbital interaction energy, ΔE_{oi}, the steric interaction energy, $\Delta E°$, and the total interaction energy, ΔE_{int}, computed for the planar and saddled conformations of H_2TPP and H_4TPP^{2+}, are plotted as a function of the tilting angle of the *meso*-phenyl groups, θ, in Figure 7. The energy decomposition analysis results for H_2TPP and H_4TPP^{2+} are given in Tables S1, S2, and S3, S4, respectively, of the Supporting Information.

As can be inferred from the curves in Figure 7, the individual energy terms for the interaction of the $(Ph^{\bullet})_4$ fragment with the porphyrin macrocycle show strikingly similar θ dependence in H_2TPP and H_4TPP^{2+}. Therefore, to simplify the discussion, we focus on the H_4TPP^{2+} results and only point out significant differences with H_2TPP.

Attractive Interactions: π Conjugation. As has been pointed out in the previous section, when the saddling is coupled with tilting of the phenyls, a considerable stabilization is achieved. This suggests that the rotation of the phenyl groups is energetically a favorable process. According to the energy decomposition displayed in Figure 7, this is fully caused by more favorable orbital interaction; compare the more negative ΔE_{oi} energies upon phenyl rotation.

The steric repulsion embodied in the $\Delta E°$ energy term only becomes more repulsive upon phenyl rotation. We will discuss the $\Delta E°$ term fully in the next section but first address the question of the electronic driving force for the rotation. What are the stabilizing orbital interactions that account for the behavior of the ΔE_{oi} term along the θ coordinate? To answer this question, we first sort out the relevant orbital interactions between the $[H_4(PyC^{\bullet})_4]^{2+}$ and $(Ph^{\bullet})_4$ fragments. These fragments set up four σ-electron-pair bonds that involve the singly occupied sp^2-like hybrids on the C_1 atoms of the phenyl radicals and the σ hybrids on the C_m atoms of the $[H_4(PyC^{\bullet})_4]^{2+}$

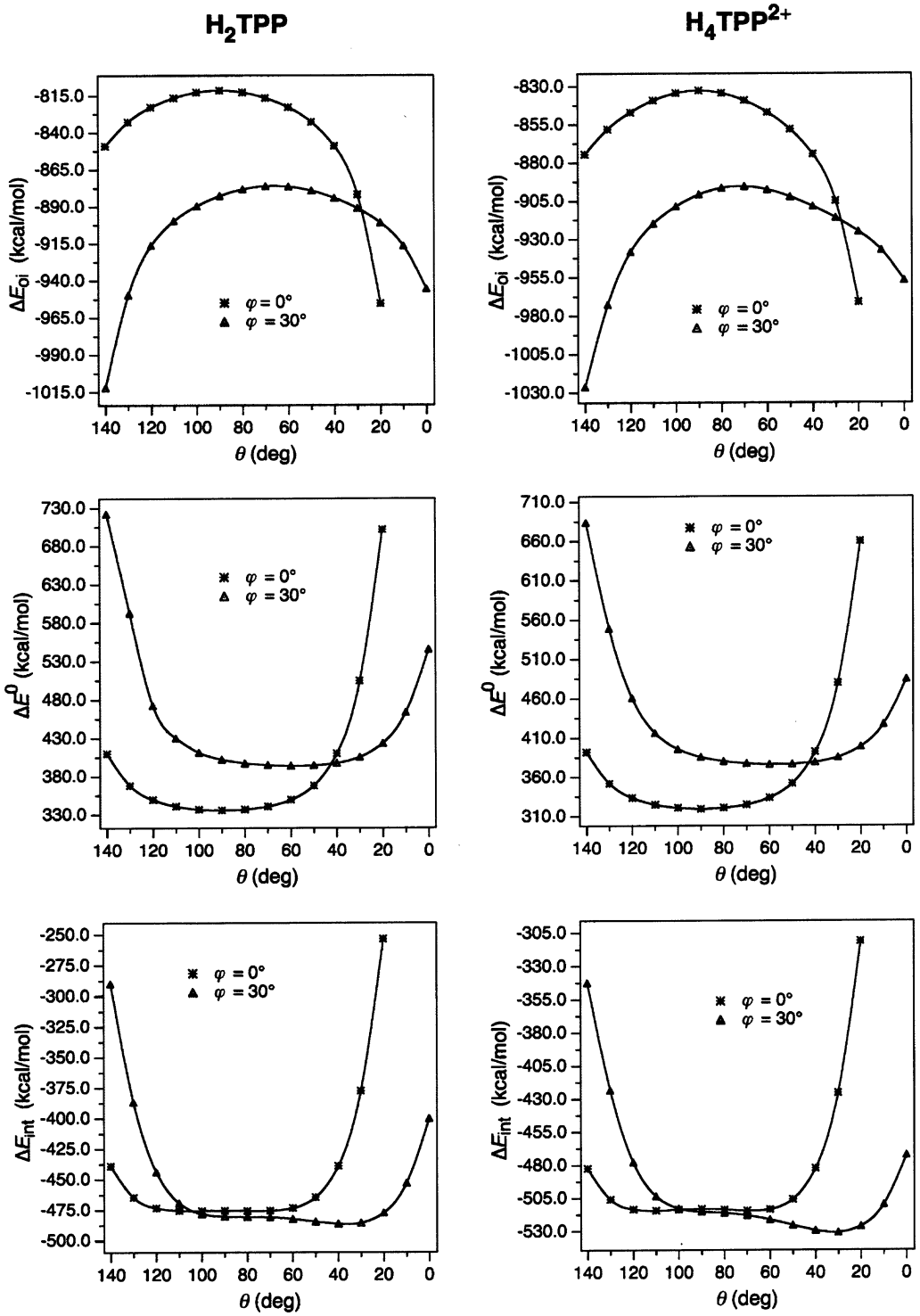

Figure 7. Variation of the energy terms along the tilting angle θ for H_2TPP and H_4TPP^{2+} in the planar ($\varphi = 0°$) and saddle ($\varphi = 30°$) conformations.

fragment. These σ-electron-pair bonds, which occur in the A_1, B_1, and E symmetries in D_{2d}, are expected to provide a contribution to the ΔE_{oi} term that is large but substantially θ-independent. This fits in with the large absolute values of the ΔE_{oi} energies in Figure 7. As for the π-type interactions, they involve the $[H_4(PyC\cdot)_4]^{2+}$ orbitals with large amplitude on the meso carbons and the $(Ph\cdot)_4$ π orbitals with large amplitude on the C_1 atoms. The pertinent $[H_4(PyC\cdot)_4]^{2+}$ molecular orbitals are the occupied $9b_2$ and unoccupied 15e and $6a_2$. As inferred from the plots of these orbitals in Figure 8, they closely resemble the G-a_{2u} (G = Gouterman), G-e_g*, and b_{1u} porphyrin (D_{4h}) orbitals, respectively. The character of these orbitals has been discussed in detail elsewhere.[42,43]

The shape of these frontier obitals follows directly from elementary orbital interaction considerations, taking the meso carbon atoms and the pyrrole rings as building blocks.

The large amplitude of the $9b_2$ (G-a_{2u}) at the meso carbons, which was a distinguishing feature of the orbital interaction scheme,[42,43] is relevant in the present context. Also, the well-understood[42,43] higher energy (ca. 2 eV) of the LUMO+1 $6a_2$ (cf. b_{1u} in the D_{4h} porphyrin) compared to the LUMO 15e (G-e_g*) will turn out to be important here.

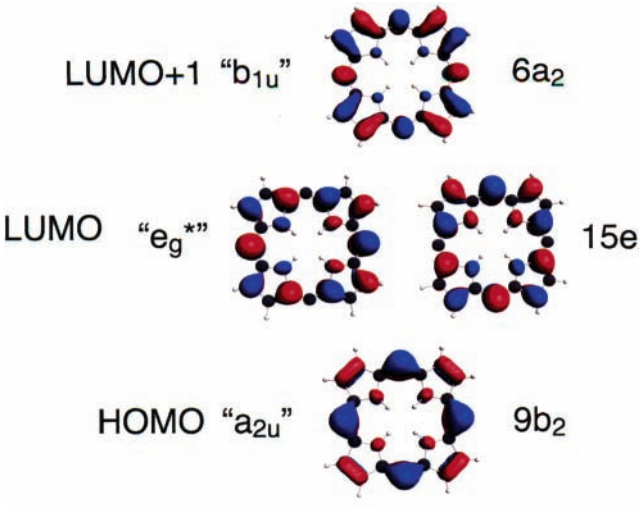

Figure 8. Frontier orbitals of $[H_4(PyC\cdot)_4]^{2+}$.

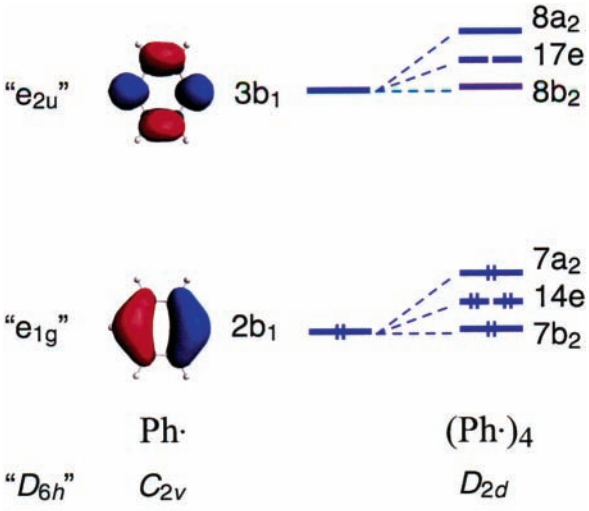

Figure 9. $(Ph\cdot)_4$ levels generated from the $2b_1$ and $3b_1$ molecular orbitals of the phenyl radical, Ph·.

The pertinent $(Ph\cdot)_4$ π orbitals are those generated from the HOMO $2b_1$ orbital of the phenyl radical (originating from one of the degenerate e_{1g} HOMO orbitals of benzene) and its LUMO $3b_1$ orbital (one of the LUMO e_{2u} orbitals of benzene). As schematically depicted in Figure 9, the $2b_1$ orbital generates the occupied $7b_2$, 14e, and $7a_2$ orbitals, and the $3b_1$ orbital generates the unoccupied $8b_2$, 17e, and $8a_2$ orbitals. The latter get, however, very little involved because of energy mismatch. The occupied orbitals of the positively charged $[H_4(PyC\cdot)_4]^{2+}$ fragment are indeed too low in energy to interact with the virtual $(Ph\cdot)_4$ orbitals. This is different in H_2TPP, as will be discussed later.

Of the occupied π levels of the $(Ph\cdot)_4$ cage, the $7b_2$ orbital interacts with the G-a_{2u}-derived $9b_2$ orbital of the $[H_4(PyC\cdot)_4]^{2+}$ fragment. This is, however, a repulsive four-electron, two-orbital interaction and contributes to the Pauli repulsion to be discussed in the next section.

The other two occupied $(Ph\cdot)_4$ molecular orbitals, $7a_2$ and 14e, have the right symmetry to interact with the unoccupied $6a_2$ and 15e orbitals of the $[H_4(PyC\cdot)_4]^{2+}$ fragment. This is the main π-conjugation interaction between the *meso*-phenyl groups and the porphyrin core. As can be inferred from Figure 10, where the plots of these fragment orbitals are displayed for the case where the interacting fragments are in the geometry that they assume in the H_4TPP^{2+} structure with $\varphi = 30°$ and $\theta = 30°$, the $7a_2$ and 14e orbitals of the phenyl cage set up π out-of-plane interactions with the $6a_2$ and 15e orbitals of the $[H_4(PyC\cdot)_4]^{2+}$ fragment, respectively.

Taking the rightmost phenyl in Figure 10, we note that it is rotated counterclockwise to smaller θ, toward the bottom right pyrrole group, which has C_β (and C_α) lowered below the porphyrin plane; compare Figure 1 (the two neighboring phenyls are rotated clockwise).

The π orbital on C_m has been tilted also to a smaller θ than 90°, so the phenyl has to rotate considerably to bring the π orbital on C_1 into reasonable overlap with the C_m π orbital. An analysis of the orbital interactions at different θ values shows that these phenylporphyrin donor−acceptor interactions are already significant at $\theta = 60°$ in the planar structure, while they switch on at somewhat smaller θ values in the saddled ($\varphi = 30°$) structure. This fits in with the fact that the saddling already tilts the C_m π orbital, as mentioned above. We also note that the ΔE_{oi} curves in Figure 7 are displaced for the saddled structure to lower θ values, with the maximum (least favorable ΔE_{oi}) not occurring at $\theta = 90°$ but at ca. $\theta = 70°$, when the phenyl plane is more nearly orthogonal to the local $C_\alpha-C_m-C_\alpha$ plane.

That the energy lowering due to π conjugation can counteract the energy cost of the saddling only at $\theta < 60°$ offers a natural explanation for the observed preponderance of the simultaneous occurrence in $[M(TPP)]^{n+}$ (M = transition metal) complexes of both a *sad* core geometry and phenyl dihedral angles smaller than 60°.[6]

The interaction with the $6a_2$ orbital of the porphyrin is weaker than that with the 15e orbital because of the higher energy of the $6a_2$ orbital. As a matter of fact, the charge transferred from the $7a_2$ and 14e molecular orbitals of the phenyl cage into the $6a_2$ and 15e orbitals of the porphyrin core, respectively, amounts to 0.07 and 0.26 electrons at $\theta = 50°$ for the saddled ($\varphi = 30°$) porphyrin, and they become 0.11 and 0.40 electrons at $\theta = 30°$ and 0.14 and 0.50 electrons at $\theta = 10°$.

It is worthwhile to mention that in H_2TPP an additional contribution to the π conjugation comes from the reverse charge-transfer interactions, i.e., porphyrin to phenyl. These mainly involve the G-a_{2u}-derived HOMO orbital of the porphyrin core, whose large amplitude at C_m was already noted. It has a_1 symmetry in the pertinent C_{2v} point group of the $[H_2(PyC\cdot)_4]$ fragment, as is the case for one of the unoccupied $(Ph\cdot)_4$ orbitals generated from the $3b_1$ orbital of the phenyl radical, the $8b_2$ orbital (in D_{2d} symmetry) of Figure 9. This interaction is not important with the $[H_4(PyC\cdot)_4]^{2+}$ fragment because the positive charge stabilizes the occupied orbitals too much, causing a too large energy mismatch with the virtuals of $(Ph\cdot)_4$.

A quantitative assessment of the role that these occupied/virtual interactions play in the ΔE_{oi} becoming increasingly stabilizing as the phenyl rings move toward the porphyrin plane is provided by the orbital interaction energy analysis that we have performed in the whole range of θ. The results for the planar porphyrin are gathered in Table 1.

As inferred from this table, the ΔE_{A_1} and ΔE_{B_1} terms, which only account for σ-pair bonds, change very little with θ, as expected. We therefore expect that the σ bonding that is present in the ΔE_E term will also vary little with θ. The variation that is visible in the ΔE_E term is therefore ascribed to the increase of π conjugation from effectively 0 kcal/mol at $\theta = 90°$ to ca. 40 kcal/mol at $\theta = 30°$. There is a much smaller effect in the A_2 symmetry due to the much higher energy of the $6a_2$ orbital (porphyrin "b_{1u}") than the 15e orbital (G-e_g*). Apart from π conjugation, there will also be some stabilizing polarization

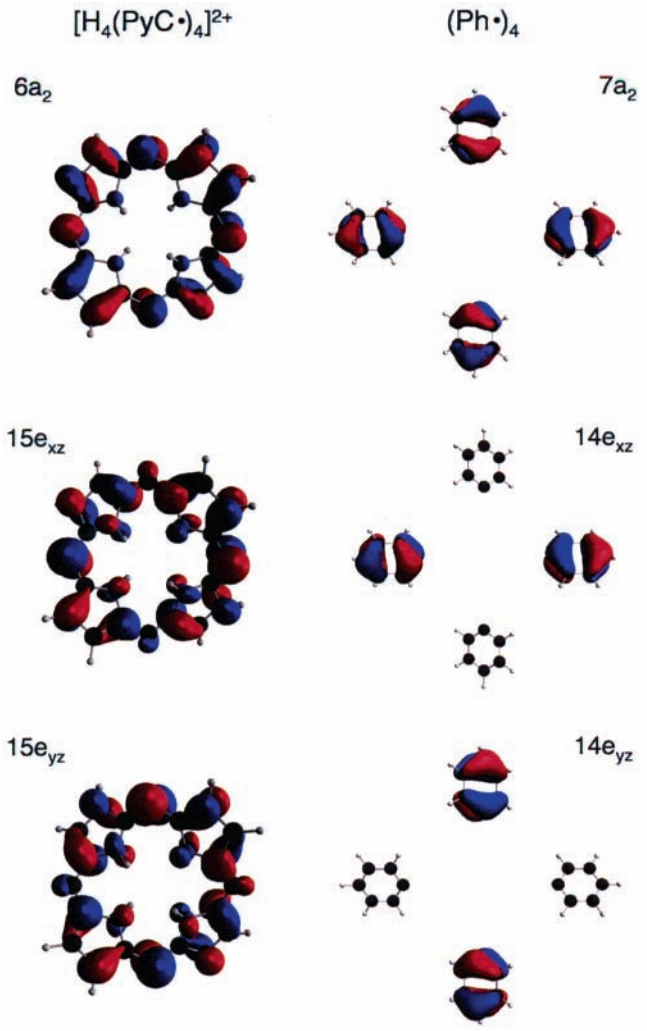

Figure 10. Plots of the $[H_4(PyC\cdot)_4]^{2+}$ $6a_2$ and 15e (left side) and $(Ph\cdot)_4$ $7a_2$ and 14e (right side) fragment orbitals. The fragments are taken in exactly the geometry they have in the H_4TPP^{2+} structure with $\varphi = 30°$ and $\theta = 30°$.

TABLE 1: Orbital Interaction Energy Analysis for the Interaction between $[H_4(PyC\cdot)_4]^{2+}$ in the Planar Conformation ($\varphi = 0°$) and the $(Ph\cdot)_4$ Cage, at Different Tilting Angles of the Phenyl Rings, θ (Energy Values in kcal/mol)

	ΔE_Γ					
θ (deg)	ΔE_{A_1}	ΔE_{A_2}	ΔE_{B_1}	ΔE_{B_2}	ΔE_E	ΔE_{oi} ($\Sigma_\Gamma \Delta E_\Gamma$)
140	−186.2	−27.6	−191.6	−24.4	−445.1	−874.5
130	−185.1	−25.0	−189.6	−22.8	−435.5	−858.0
120	−184.4	−23.0	−189.1	−21.9	−428.6	−847.0
110	−184.2	−21.6	−188.5	−21.5	−423.4	−839.2
100	−184.0	−20.7	−188.4	−21.3	−420.0	−834.4
90	−184.0	−20.4	−188.3	−21.2	−418.8	−832.7
80	−184.0	−20.7	−188.4	−21.3	−420.0	−834.4
70	−184.2	−21.6	−188.5	−21.5	−423.4	−839.2
60	−184.4	−23.0	−189.1	−21.9	−428.6	−847.0
50	−185.1	−25.0	−189.6	−22.8	−435.5	−858.0
40	−186.2	−27.6	−191.6	−24.4	−445.1	−874.5
30	−189.0	−31.5	−194.8	−28.4	−461.2	−904.9
20	−196.1	−39.5	−202.7	−37.6	−495.1	−971.0

(occupied/virtual mixing on one fragment) contributing to ΔE_{A_2}. We finally have the ΔE_{B_2} term, which incorporates the small π conjugation occurring in that symmetry in the form of porphyrin ($9b_2$) to phenyl ($8b_2$) charge transfer and, of course, includes some polarization. The increase of this π conjugation when θ is lowered from 90° is even smaller than the phenyl-porphyrin π conjugation in the A_2 symmetry.

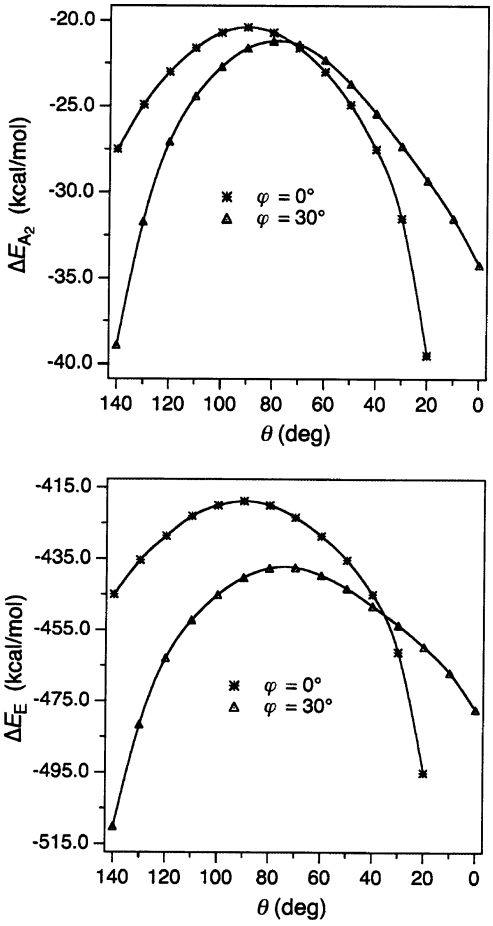

Figure 11. Variation of the ΔE_{A_2} and ΔE_E terms along the tilting angle θ for H_4TPP^{2+} in the planar ($\varphi = 0°$) and saddle ($\varphi = 30°$) conformations.

TABLE 2: Orbital Interaction Energy Analysis for the Interaction between $[H_4(PyC\cdot)_4]^{2+}$ in the Saddle Conformation ($\varphi = 30°$) and the $(Ph\cdot)_4$ Cage, at Different Tilting Angles of the Phenyl Rings, θ (Energy Values in kcal/mol)

	ΔE_Γ					
θ (deg)	ΔE_{A_1}	ΔE_{A_2}	ΔE_{B_1}	ΔE_{B_2}	ΔE_E	ΔE_{oi} ($\Sigma_\Gamma \Delta E_\Gamma$)
140	−201.4	−38.9	−238.0	−37.8	−510.2	−1026.3
130	−196.2	−31.7	−232.7	−30.4	−481.5	−972.5
120	−193.2	−27.1	−229.5	−25.6	−462.9	−938.3
110	−191.9	−24.4	−228.0	−23.4	−452.2	−919.9
100	−191.3	−22.6	−227.0	−22.4	−445.2	−908.5
90	−190.9	−21.6	−226.1	−22.0	−440.2	−900.8
80	−190.6	−21.2	−225.3	−21.9	−437.5	−896.5
70	−190.2	−21.4	−224.5	−22.0	−437.4	−895.5
60	−189.9	−22.3	−223.8	−22.1	−439.5	−897.6
50	−189.6	−23.7	−223.1	−22.4	−443.4	−902.2
40	−189.3	−25.4	−222.7	−22.9	−448.2	−908.5
30	−189.2	−27.3	−222.4	−23.6	−453.6	−916.1
20	−189.2	−29.3	−222.5	−24.4	−459.7	−925.1
10	−189.7	−31.5	−223.2	−25.9	−467.0	−937.3
0	−191.4	−34.2	−225.4	−28.4	−477.4	−956.8

It is interesting to compare to the saddled structure, for which the energy analysis is given in Table 2. In Figure 11, the ΔE_{A_2} and ΔE_E terms are plotted as a function of θ for both the saddled and planar structures.

Whereas for the planar structure the ΔE terms exhibit monotonic decreases (more stabilization) when θ is decreased from 90°, the ΔE_E term more strongly than the ΔE_{A_2} term, for

SCHEME 1

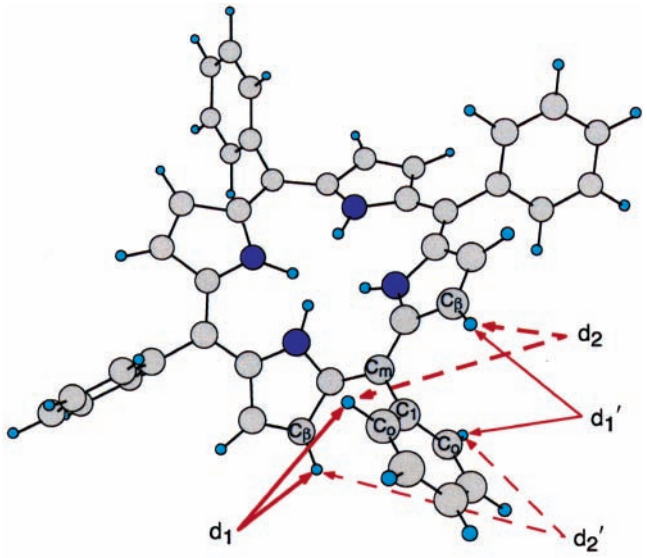

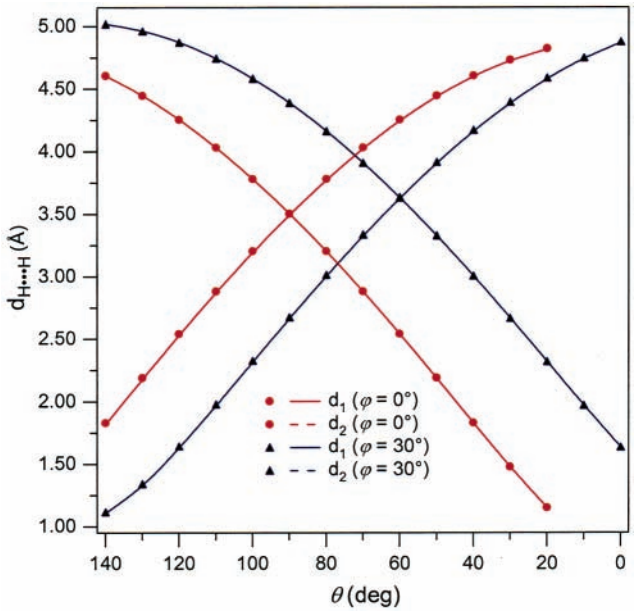

Figure 12. Variation of the $H_\beta\cdots H_o$ distances d_1 (drawn lines) and d_2 (broken lines) along the tilting angle θ, for the planar ($\varphi = 0°$, red curves) and saddled ($\varphi = 30°$, blue) conformations of H_4TPP^{2+}.

the saddled structure, the stabilization first diminishes. This is in accordance with the observation above that the phenyl plane first will rotate to a more orthogonal position with respect to the local $C_\alpha-C_m-C_\alpha$ plane, so that the π-conjugation stabilization will decrease. The energy values reported in Tables 1 and 2 clearly indicate that the behavior of the ΔE_{oi} term along θ is dominated by the ΔE_{A_2} and ΔE_E terms, in both the planar and saddled conformations. The ΔE_{A_2}, ΔE_E, and ΔE_{oi} curves show indeed a similar shape.

Repulsive Interactions. Because as we have seen the π conjugation tries to pull the phenyl plane to $\theta = 0°$ (i.e., in the plane of the porphyrin macrocycle), the fact that small θ angles are not found must be caused by a counteracting force. As expected, the $\Delta E°$ term, incorporating the steric repulsion, increases when the phenyl rings are rotated toward the porphyrin plane. In the planar system, the $\Delta E°$ curve is, of course, symmetric around $\theta = 90°$ (see Figure 7). For the saddled system, the repulsion increases more rapidly when the phenyls are rotated toward the upward-tilted pyrrole, which with our convention for θ corresponds to $\theta > 90°$ (see Figure 1), and increases later (i.e., after rotation over a larger angle) when the phenyls are rotated toward the downward-tilted pyrrole ring ($\theta < 90°$). Equivalently, the whole $\Delta E°$ curve in Figure 7 is somewhat shifted for the saddled system toward lower θ values. We note that the minimum in the $\Delta E°$ curves is rather shallow. This implies that the phenyls can rotate without much energy penalty around the preferred orientation by some $\pm 30°$, with the steric repulsion from "hitting" the pyrrole rings only providing a repulsive "wall" at larger rotation angles. The behavior of the $\Delta E°$ curves in Figure 7 is dominated by the Pauli repulsion term. The ΔE_{elstat} values gathered in Tables S3 and S4 in the Supporting Information indicate that this term provides a nearly constant stabilizing contribution to the $\Delta E°$ term over a wide range of θ. From $\theta = 20°$ (40° in the case of $\varphi = 0°$) onward, its contribution becomes increasingly stabilizing, but such small values of θ are not reached because of the concomitantly large increase of the destabilizing ΔE_{Pauli} term that prevails over ΔE_{elstat} at all angles.

To rationalize the behavior of the $\Delta E°$ curves in Figure 7, we note that the main contribution to the Pauli repulsion comes from the interactions between the ortho carbon−hydrogen bonds of the phenyls, C_o-H_o, and the $C_\beta-H_\beta$ σ bonds of the two neighboring pyrrole rings (see Scheme 1). When the porphyrin core is planar and the phenyls are orthogonal to the porphyrin plane, the two distances d_1 and d_2 are equal and the two interactions for one C_o-H_o σ-bond orbital (there are 16 such interactions in total) will equally contribute to the Pauli repulsion term. This is not so, however, when $\theta < 90°$ or when the porphyrin core is saddled. For a saddled porphyrin at $\theta = 90°$, each C_o-H_o σ-bond orbital will have a short distance (indicated as d_2, drawn line in Scheme 1 for the C_o-H_o bond above the porphyrin plane) to the pyrrole to the right with the $C_\beta-H_\beta$ bonds tilted upward and a long distance d_1 (dashed line) for the downward-tilted pyrrole to the left. Of course, the C_o-H_o σ-bond orbital at the down side will have a short distance (d_2') and a long distance (d_1') to just the reverse pyrroles; see the thin red lines in Scheme 1.

In Figure 12, the d_1 and d_2 $H_\beta\cdots H_o$ distances are plotted as a function of θ, for the planar ($\varphi = 0°$, red lines) and saddled ($\varphi = 30°$, blue lines) conformations of H_2TPP^{2+}. When the porphyrin core is planar, d_1 and d_2 coincide and are quite long at $\theta = 90°$. Upon tilting of the phenyl rings, d_2 elongates and d_1 shortens, becoming at $\theta = 50°$ ~2.3 Å, only 0.3 Å longer than the sum of the hydrogen van der Waals radii.[44] This fits in with the rapid rise of the $\Delta E°$ curve from $\theta = 50°$ downward. In the saddled structure, d_2 is at $\theta = 90°$ much shorter than d_1 and considerably shorter indeed than that in the planar structure (2.70 vs 3.40 Å). This explains why at $\theta = 90°$ the $\Delta E°$ term is in the saddled structure significantly more repulsive than that in the planar one (see Figure 7).

From $\theta = 90°$ downward, d_2 elongates and d_1 shortens. Still, d_1 is at all angles ~1 Å longer than that in the planar structure, and at $\theta = 10°$, it is still longer than the sum of the hydrogen van der Waals radii. This fully explains the much weaker steric repulsion for the saddled structure, which allows the phenyl ring to rotate to much smaller θ angles before hitting the repulsive wall.

An additional, minor contribution to the Pauli repulsion comes from the four-electron, two-orbital interaction between the occupied $(P^\bullet)_4$-$7b_2$ and $[H_4(PyC^\bullet)_4]^{2+}$-$9b_2$ orbitals, mentioned in the previous section. This is quantitatively less important than the repulsion with the pyrrole rings, but it has important spectroscopic effects because the considerable overlap between

these orbitals, which have significant amplitude at the C_m and C_1 atoms, leads to destabilization of the antibonding combination.[25]

Total Interaction Energy. We finally consider the effect of steric repulsion and orbital interaction (π conjugation) together. The resulting ΔE_{int} curves in the bottom panel of Figure 7 demonstrate quite strikingly how shallow the minimum of the total energy becomes. Concentrating on the lowering of θ to small values, we see that the saddled structure allows θ to become much smaller than the planar structure, and because of the increase in stabilizing π conjugation at those small angles, there occurs a clear minimum in ΔE_{int} at $\theta \sim 30°$. If one considers the combined motion of saddling and phenyl ring tilting, it is clear that when we would forget about the energy cost of the saddling, the system would distort to the saddled and tilted configuration. When we add to the total energy in Figure 7, the energy cost of the saddling, which at $\varphi = 30°$ is slightly less than 20 kcal/mol for H_2TPP, the distortion will just not be favorable for H_2TPP. However, evidently the system has become very soft toward this deformation, and a small additional effect, such as that provided by the inner hydrogen repulsion in H_4TPP^{2+}, where the saddling is favorable from 0° to 40°, will firmly send the system into the combined saddled and tilted distortion.

The Synergic Mechanism at Work

We have quantified the energetic effects of the saddling distortion and the *meso*-phenyl ring twisting, and we have elucidated the electronic structure origin of these energetic effects. The conclusion is that the variety of observed structures of *meso*-aryl-substituted porphyrins can be rationalized from the point of view that the system is soft toward deformation along a coupled distortion mode. Systems with just *meso*-aryl substitution, like H_2TPP and H_2TPyP, will not yet distort, but a slight additional driving force will tip the balance. It is interesting to review some of the structural data from this angle.

Diacids. Nonplanar distortion is realized by the addition of two protons to the pyrrolic nitrogens of the porphyrin core to form the diacid. As revealed by X-ray crystallography,[14−16,20,21,24,45,46] porphyrin diacids typically have nonplanar structures with mainly saddle-type distortions, with a small to negligible sideways tilt (ruffling) of the pyrrole rings *superimposed* on the large vertical tilt. The deviation from planarity for diacids bearing *meso*-aryl substituents, such as H_4TPP^{2+} and H_4TPyP^{2+},[14,16] is much more pronounced than that for other diacids, such as H_4OEP^{2+}.[16,20] For instance, in H_4TPP^{2+} derivatives,[14,16,21] the observed average tilt of the pyrrole rings, φ, ranges between 28 and 33°. This is to be compared to $\varphi \sim 14°$ seen in H_4OEP^{2+} derivatives.[16,20] The larger "flexibility" of H_4TPP^{2+} with respect to H_4OEP^{2+} derivatives has been explained so far in terms of the former being more susceptible than the latter to packing-induced conformational distortions, in particular rotation of the phenyl groups, which would induce stronger saddling for steric reasons.[16] Our theoretical analysis clearly shows that the relatively large distortion of *meso*-aryl-substituted porphyrins has, instead, intrinsic electronic reasons. The H_4P^{2+} and H_4TPP^{2+} PECs in Figure 2 show that, in order to relieve the steric repulsion of the inner hydrogens, a saddling of 10−15° is sufficient. This accounts perfectly for the low saddling angle of $\varphi \sim 14°$ seen in H_4OEP^{2+} derivatives. The $\Delta E°$ curves in Figure 7 show, by interpolation between the $\varphi = 0°$ and $\varphi = 30°$ cases, that in *meso*-phenyl-substituted systems at $\varphi = 15°$ there is no energy gain for steric reasons to go to a smaller θ angle than ca. 75°. The fact that the saddling is typically much stronger and the θ angle much sharper is entirely due to the electronic synergic effects we have pointed out.

Peripheral Congestion. It is well-known that neutral *meso*-arylporphyrins can undergo significant saddling distortion upon the introduction of β substituents. A considerable body of information has now been accumulated for such sterically overloaded porphyrins.[5,13] The most prominent examples are the dodeca-substituted porphyrins, H_2OETPP,[9,22] H_2DDPP,[10] and H_2Br_8TPP,[8] which show highly saddled conformations ($\varphi \sim 30°$). The driving force to activate the synergic mechanism we have pointed out comes in these systems from the repulsion between the peripheral substituents. On the basis of our theoretical data, we cannot quantify the degree of saddling distortion necessary to relieve the peripheral steric congestion for the various types of substituents at C_β, but when the steric requirements allow the phenyl rings to rotate to sufficiently small angles, the electronic stabilization upon phenyl ring rotation will be effective and make the system very soft toward the concerted saddling/rotation motion. This is apparently the case; the average phenyl−porphyrin dihedral angle in these systems is hardly larger than 45°.

The saddling of $\varphi = 30°$ in the dodeca-substituted *meso*-phenylporphyrins is actually comparable to that seen in the *meso*-aryl-containing diacids. Understandably, the diacids of these overloaded porphyrins show even larger saddle distortions ($\varphi \sim 40°$).[23,24]

***meso*-Alkyl Substitution.** We comment on the saddle distortions observed in *meso*-alkyl-substituted porphyrin diacids. Despite the absence of *meso*-aryl substituents, these diacids show saddling distortions comparable to or even larger than those observed in *meso*-aryl-containing diacids, with the actual degree of saddling increasing with the size of the alkyl groups.[47] Of course, the synergic mechanism we have pointed out does not apply in this case. However, the large saddling of these diacids can still be rationalized without invoking external forces. In fact, the energy cost of the saddling is compensated for, in part, by the relief of the Pauli repulsion of the inner hydrogens (which we have seen would lead to ca. ∼15° of saddling). That the saddling also in this case becomes much larger must be due to the relief of steric hindrance between the *meso*-alkyl substituents and the flanking pyrrole rings, a totally different cause than that in the case of *meso*-aryl substitution.

Correlation of the Phenyl Tilt Angle and Saddling Angle. We have noted in the Introduction that a number of structural studies on *meso*-aryl-containing diacids[6,7,16] have clearly demonstrated that there is a correlation between the magnitude of the saddle distortion and decreasing porphyrin−aryl dihedral angles, θ. It is interesting to compare the strongly saddled/rotated $[H_4TPP](ClO_4)_2$ where the average porphyrin−aryl dihedral angle, θ, is 27(2)° and $|\Delta C_\beta|$ amounts to 0.93(6) Å,[16] with $[H_4TMP](ClO_4)_2$ where the steric bulk of the mesityl substituents prevents the porphyrin−aryl dihedral angle from becoming smaller than ∼60°. In that case, the synergic mechanism cannot become very effective, and the saddling remains limited ($|\Delta C_\beta| = 0.67$ Å).[16] The observed $|\Delta C_\beta|$ value is only 0.20 Å larger than that in $[H_4OEP](ClO_4)_2$,[16] a diacid which lacks aryl groups. In fact, in ref 16 a series of 2,6-disubstituted phenyls are considered, and it has been noticed that the flexibility of the tetraarylporphyrin diacids decreases as the steric bulk of the 2,6 subsituents increases. At the same time, it has been noted that the θ angle remains large, which must have steric reasons. When θ is large, the synergic mechanism cannot become operative, so the lack of flexibility is fully consistent with and

explained by our results. Interestingly, an argument based purely on steric hindrance would indicate the reverse to happen: if the saddling is driven by relief of steric hindrance with the *meso*-aryl groups, larger steric bulk of the 2,6 substituents would be expected to lead to *stronger* saddling to avoid the steric repulsion.

Supporting Information Available: Energy decomposition analysis results for H_2TPP (Tables S1 and S2) and H_4TPP^{2+} (Tables S3 and S4). This material is available free of charge via the Internet at http://pubs.acs.org.

References and Notes

(1) Shelnutt, J. A.; Song, X.-Z.; Ma, J.-G.; Jia, S.-L.; Jentzen, W.; Medforth, C. J. *Chem. Soc. Rev.* **1998**, *27*, 31.
(2) Mazzanti, M.; Marchon, J.-C.; Shang, M.; Scheidt, W. R.; Jia, S.; Shelnutt, J. A. *J. Am. Chem. Soc.* **1997**, *119*, 12400.
(3) Muzzi, C. M.; Medforth, C. J.; Smith, K. M.; Jia, S.-L.; Shelnutt, J. A. *Chem. Commun.* **2000**, 131.
(4) Gazeau, S.; Pécaut, J.; Haddad, R. E.; Shelnutt, J. A.; Marchon, J.-C. *Eur. J. Inorg. Chem.* **2002**, 2956.
(5) Senge, M. O. In *The Porphyrin Handbook*; Kadish, K. M., Smith, K. M., Guilard, R., Eds.; Academic Press: Boston, 2000; Vol. 1; p 239.
(6) Scheidt, W. R.; Lee, Y. J. *Struct. Bonding* **1987**, *64*, 1.
(7) Munro, O. Q.; Bradley, J. C.; Hancock, R. D.; Marques, H. M.; Marsicano, F.; Wade, P. W. *J. Am. Chem. Soc.* **1992**, *114*, 7218.
(8) Spyroulias, G. A.; Despotopoulos, A. P.; Raptopoulou, C. P.; Terzis, A.; de Montauzon, D.; Poiblanc, R.; Coutsolelos, A. G. *Inorg. Chem.* **2002**, *41*, 4648.
(9) Barkigia, K. M.; Berber, M. D.; Fajer, J.; Medforth, C. J.; Renner, M. W.; Smith, K. M. *J. Am. Chem. Soc.* **1990**, *112*, 8851.
(10) Medforth, C. J.; Senge, M. O.; Smith, K. M.; Sparks, L. D.; Schelnutt, J. A. *J. Am. Chem. Soc.* **1992**, *114*, 9859.
(11) Barkigia, K. M.; Renner, M. W.; Ferunlid, L. R.; Medforth, C. J.; Smith, K. M. *J. Am. Chem. Soc.* **1993**, *115*, 3627.
(12) Nurco, D. J.; Medforth, C. J.; Forsyth, T. P.; Olmstead, M. M.; Smith, K. M. *J. Am. Chem. Soc.* **1996**, *118*, 10918.
(13) Medforth, C. J.; Haddad, R. E.; Muzzi, C. M.; Dooley, N. R.; Jaquinod, L.; Shyr, D. C.; Nurco, D. J.; Olmstead, M. M.; Smith, K. M.; Ma, J.-G.; Shelnutt, J. A. *Inorg. Chem.* **2003**, *125*, 1253.
(14) Stone, A.; Fleischer, E. B. *J. Am. Chem. Soc.* **1968**, *90*, 2735.
(15) Senge, M. O.; Kalisch, W. W. *Z. Naturforsch.* **1999**, *54b*, 943.
(16) Cheng, B.; Munro, O. Q.; Marques, H. M.; Scheidt, W. R. *J. Am. Chem. Soc.* **1997**, *119*, 10732.
(17) Hamor, M. J.; Hamor, T. A.; Hoard, J. L. *J. Am. Chem. Soc.* **1964**, *86*, 1938.
(18) Senge, M. O.; Kalish, W. W. *Inorg. Chem.* **1997**, *36*, 6103.
(19) Kano, K.; Fukuda, K.; Wakami, H.; Nishiyabu, R.; Pasternack, R. F. *J. Am. Chem. Soc.* **2000**, *122*, 7494.
(20) Nguyen, L. T.; Senge, M. O.; Smith, K. M. *Tetrahedron Lett.* **1994**, *35*, 75.
(21) Navaza, A.; deRango, C.; Charpin, P. *Acta Crystallogr., Sect. C* **1983**, *C39*, 1625.
(22) Sparks, L. D.; Medforth, C. J.; Park, M.-S.; Chamberlain, J. R.; Ondrias, M. R.; Senge, M. O.; Smith, K. M.; Schelnutt, J. A. *J. Am. Chem. Soc.* **1993**, *115*, 581.
(23) Senge, M. O.; Forsyth, T. P.; Nguyen, L. T.; Smith, K. M. *Angew. Chem., Int. Ed. Engl.* **1994**, *33*, 2485.
(24) Barkigia, K. M.; Fager, J.; Berber, M. D.; Smith, K. M. *Acta Crystallogr., Sect. C* **1995**, *C51*, 511.
(25) Rosa, A.; Ricciardi, G.; Baerends, E. J.; Romeo, A.; Monsù Scolaro, L. *J. Phys. Chem. A* **2003**, *107*, 11468.
(26) *Amsterdam Density Functional Program*; Theoretical Chemistry, Vrije Universiteit: Amsterdam, The Netherlands, http://www.scm.com.
(27) te Velde, G.; Bickelhaupt, F. M.; Baerends, E. J.; Fonseca Guerra, C.; van Gisbergen, S. J. A.; Snijders, J. G.; Ziegler, T. *J. Comput. Chem.* **2001**, *22*, 931.
(28) Vosko, S. H.; Wilk, L.; Nusair, M. *Can. J. Phys.* **1980**, *58*, 1200.
(29) Becke, A. *Phys. Rev. A* **1988**, *38*, 3098.
(30) Perdew, J. P. *Phys. Rev. B* **1986**, *33*, 8822 (Erratum: *Phys. Rev. B* **1986**, *34*, 7406).
(31) Bickelaupt, F. M.; Baerends, E. J. In *Reviews in Computational Chemistry*; Lipkowitz, K. B., Boyd, D. R., Eds.; Wiley: New York, 2000; Vol. 15; p 1.
(32) Morokuma, K. *J. Chem. Phys.* **1971**, *55*, 1236.
(33) Ziegler, T.; Rauk, A. *Theor. Chim. Acta* **1977**, *46*, 1.
(34) Fujimoto, H.; Osamura, Y.; Minato, T. *J. Am. Chem. Soc.* **1978**, *100*, 2954.
(35) Kitaura, K.; Morokuma, K. *Int. J. Quantum Chem.* **1976**, *10*, 325.
(36) van den Hoek, P. J.; Kleyn, A. W.; Baerends, E. J. *Comments At. Mol. Phys.* **1989**, *23*, 93.
(37) Bickelhaupt, F. M.; Nibbering, N. M. M.; van Wezenbeek, E. M.; Baerends, E. J. *J. Phys. Chem.* **1992**, *96*, 4864.
(38) Silvers, S.; Tulinsky, A. *J. Am. Chem. Soc.* **1967**, *89*, 3331.
(39) Hoard, J. L. *Science* **1971**, *174*, 1295.
(40) Hoard, J. L. In *Porphyrins and Metalloporphyrins*; Smith, K. M., Ed.; Elsevier: New York, 1975; p 317.
(41) Sessler, J. L.; Johnson, M. R.; Creager, S. E.; Fettinger, J. C.; Ibers, J. A. *J. Am. Chem. Soc.* **1990**, *112*, 9310.
(42) Rosa, A.; Ricciardi, G.; Baerends, E. J.; van Gisbergen, S. J. A. *J. Phys. Chem. A* **2001**, *105*, 3311.
(43) Baerends, E. J.; Ricciardi, G.; Rosa, A.; van Gisbergen, S. J. A. *Coord. Chem. Rev.* **2002**, *230*, 5.
(44) Bondi, A. *J. Phys. Chem.* **1964**, *68*, 441.
(45) Sheldrick, W. S. *J. Chem. Soc., Perkin Trans.* **1976**, *2*, 453.
(46) Cetinkaya, E.; Johnson, A. W.; Lappert, M. F.; McLaughlin, G. M.; Muir, K. W. *J. Chem. Soc., Dalton Trans.* **1974**, 1237.
(47) Senge, M. O. *Z. Naturforsch.* **2000**, *55b*, 336.